

# The chemical basis of zebra rock patterning

Matthew Walker \*

**Abstract** Zebra rock is a strikingly patterned siltstone found exclusively in the East Kimberley region of northwestern Australia. Its features can include centimetre-scale stripes, spots, pillars and rods rich in hematite distributed throughout a bed of silica-rich clay, all of which can be exhibited even in the same basin of rock. The exact mechanism which forms these patterns is a subject of ongoing research. Of several proposals in previous studies, the two most prominent theories are redoximorphic banding in acid-sulfate soils, and Liesegang banding in an acidic hydrothermal system. In this report, we consider the former. A reaction-diffusion model is constructed consisting of the significant chemical reactions occurring in this system, which is catalysed by a population of acidophilic microbes. It may be shown that this model can exhibit Turing instability, and the resulting patterns that eventuate share a remarkable resemblance with the rock.

## 1 Introduction

Zebra rock is a patterned siltstone, distinguished by its 2-10 cm-scale brown banding of hematite throughout an ivory coloured, quartz-rich clay composed of kaolinite, dickite and alunite (see Fig. 1). It has only been found in small outcrops in the East Kimberley region of Western Australia. The mystery surrounding zebra rock pattern formation has puzzled geochemists since its first mention in the scientific literature in 1924. The patterns are too rhythmic to be formed by sedimentary layering of soil; this has invited a host of alternative explanations, varying from the

---

Matthew Walker  
The University of Melbourne, Australia  
e-mail: walkerm4@student.unimelb.edu.au

\* This report presents the results of a project undertaken by the author at the Matrix Workshop *Instabilities in Porous Media*, April 3-23, 2024, under the supervision of A/Prof. Anja Slim (Monash University).

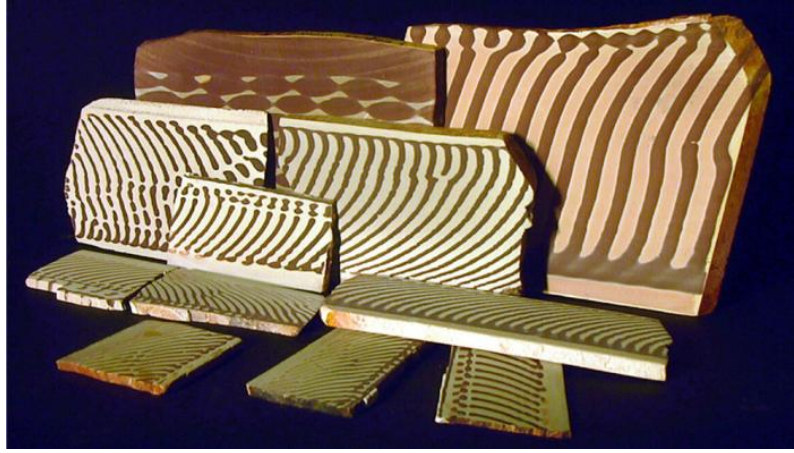


**Fig. 1** The myriad styles of patterning exhibited in zebra rock. Photograph by Geoff Deacon, courtesy of the Western Australian Museum.

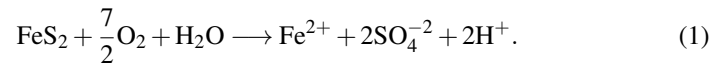
accumulation of ferruginous minerals in ripple troughs during tidal events [6], to the magnetism of the hematite bands and their self-organisation [1]. Current evidence suggests that two major geological events contributed to the creation of the rock [3]. The first event, placed at  $\sim 600$  million years ago, was the tidal infiltration of pyrite-rich soil with groundwater, which oxidised the pyrite crystals releasing  $\text{Fe}^{2+}$  and  $\text{H}^+$  ions into the system. The ambient temperature during this regime was around 25 degrees Celsius. As often occurs presently in acid-mine drainage systems, the oxidation process kicked off a chain of reactions; the pH drops to around 3-4, which allows the self-oxidation of the newly released  $\text{Fe}^{2+}$  ions to form  $\text{Fe}^{3+}$  ions. This self-oxidation of  $\text{Fe}^{2+}$  ions is the rate-limiting step in this system. The  $\text{Fe}^{3+}$  ions then assist in the oxidation of pyrite crystals. The excess  $\text{Fe}^{3+}$  ions then hydrolyze with the excess groundwater, forming ferric hydroxide ( $\text{Fe}(\text{OH})_3$ ) precipitate. The second event was a dramatic raising of temperature (possibly magmatic) to  $\sim 200$  degrees Celsius, about  $\sim 510$  million years ago, creating an acidic hydrothermal system. Such an event would provide the environment required to convert the meta-stable ferric hydroxide into the hematite within the brown banding. This event also provides conditions for high-sulfidation epithermal alteration, which could have incited additional pyrite formation, and caused the alteration of aluminosilicates responsible for the kaolinite, dickite and alunite concentrations in the light areas. Despite both of these processes having evidence of contributing to the formation of zebra rock, the exact mechanism which creates the patterns, and the time when this mechanism occurred, has yet to be determined. Liesegang banding has been touted as a potential solution, and it has been shown that its occurrence is possible during either the waterlogged acid-sulfate soil event or the hydrothermal alteration event [2].

An alternative mechanism proposed in this report is that the pattern was initialised during the acid-sulfate soil stage, wherein bands of ferric hydroxide were

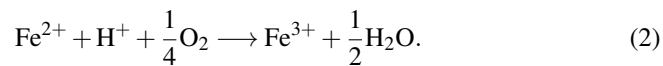
formed by a diffusion-driven instability known as a Turing instability [11]. Here,  $\text{Fe}^{2+}$  and  $\text{H}^+$  play the role of the activator inhibitor pair;  $\text{H}^+$  inadvertently activates the release of  $\text{Fe}^{2+}$  ions through the creation of  $\text{Fe}^{3+}$  ions, while  $\text{Fe}^{2+}$  inhibits the growth of  $\text{H}^+$ . The role of the hydrothermal event which happened afterwards then was only in transitioning the ferric hydroxide into hematite, and finalising the structure of the ambient aluminosilicate material, rather than contributing to pattern formation. Our model also includes the effects of acidophilic bacteria, which oxidise the  $\text{Fe}^{2+}$  ions and thus play an important role in speeding up the rate-limiting step in very acidic conditions. There are many species of these acidophilic bacteria, but the most prominent of them in this environment are hypothesised to have been *acidithiobacillus ferrooxidans* and *acidithiobacillus thiooxidans*. Each species of these bacteria have different motility properties, and  $\text{Fe}^{2+}$  or  $\text{Fe}^{3+}$  may be toxic to some, but they all do fundamentally the same thing; oxidise  $\text{Fe}^{2+}$  into  $\text{Fe}^{3+}$  ions [10].

## 2 Geochemical background

In this section, we describe the chemical processes behind the formation of the ferric hydroxide precipitate. The initial infiltration of the pyrite-rich soil with groundwater begins to oxidise the pyrite crystals and releases  $\text{Fe}^{2+}$  ions into the soil-water system, as well as increasing the acidity. This reaction is described by the equation



It plays the important role of initialising the reaction chain, releasing the  $\text{Fe}^{2+}$  and  $\text{H}^+$  in solution. This is its only role, however; the rate of this reaction is much slower than the following reactions, and is ignored in further analysis. The soil is now waterlogged, and we assume that  $\text{O}_2$  and  $\text{H}_2\text{O}$  exist in excess. The  $\text{Fe}^{2+}$  in solution then self-oxidises to form  $\text{Fe}^{3+}$  ions, according to the equation



This is the rate-limiting step, as  $\text{Fe}^{3+}$  ions are required in solution to create the precipitate. This reaction is complex and depends on many factors, such as temperature and pH [2], but for our regime of about 25 degrees and pH ranges of around 3-4, the rate equation

$$\frac{d[\text{Fe}^{3+}]}{dt} = k_1 \frac{[\text{Fe}^{2+}]}{[\text{H}^+]} \quad (3)$$

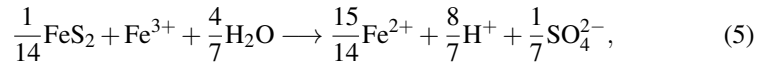
describes this reaction well enough. We note that the reaction actually shuts down at low pH, which is less than ideal for a rate-limiting step in an acidic chemical system. In fact, even at a 'low' pH of only 3.5, this reaction is two orders of magnitude lower

than the other reactions in this system. However, if we consider the presence of acidophilic bacteria, the reaction will be catalysed at low pH as the bacteria oxidise the  $\text{Fe}^{2+}$  ions to create  $\text{Fe}^{3+}$  ions according to the rate equation

$$\frac{d[\text{Fe}^{3+}]}{dt} = k_m [\text{Fe}^{2+}] [\text{H}^+] M, \quad (4)$$

where  $M$  denotes the (continuum) concentration of microbes. As many species of these microbes may exist,  $M$  just considers the population of all acidophilic microbes and analyses the general, bulk behaviour of them. The microbes essentially 'pick up the slack' of the rate-limiting reaction in very acidic conditions and allow the cycle of reactions to continue.

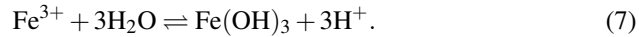
Now, the  $\text{Fe}^{3+}$  in solution can take on two possible pathways; either it oxidises the surface of the pyrite crystals and releases more  $\text{Fe}^{2+}$ , or precipitates into ferric hydroxide. The pathway taken depends on various factors. If the  $\text{Fe}^{3+}$  is saturated in the solution, then it begins to form the precipitate. Otherwise, it diffuses around until it collides with pyrite crystals and oxidises them. The oxidation reaction has equation



with rate of reaction

$$\frac{d[\text{Fe}^{3+}]}{dt} = -k_s [\text{Fe}^{3+}]. \quad (6)$$

The rate constant  $k_s$  is relatively large and so this reaction happens almost instantaneously (with respect to the characteristic time scale of the other reactions). However, because  $\text{Fe}^{3+}$  must collide with a pyrite crystal in order for this reaction to occur, the rate of reaction in this specific system is actually on the order of the time scale for  $\text{Fe}^{3+}$  to diffuse the average length between pyrite crystals. This averaging procedure places its rate at the same order of magnitude as the other reactions. Finally, the precipitation reaction which transforms  $\text{Fe}^{3+}$  into ferric hydroxide  $\text{Fe}(\text{OH})_3$  is given below:



This reaction is reversible in the acid-sulfate soil regime. This reaction will occur in the forward direction if the amount of  $\text{Fe}^{3+}$  is past its saturation threshold. It occurs in the backward direction if the pH is lower than 3.5. A usable form for the rate of this reaction was not found in the literature, and rather, the rate of reaction is modelled as

$$\begin{aligned} \frac{d[\text{Fe}_{\text{prec}}]}{dt} = & -p^- [\text{Fe}_{\text{prec}}] \left( [\text{H}^+] - [\text{H}^+]_{\text{prec}} \right) \theta \left( [\text{H}^+] - [\text{H}^+]_{\text{prec}} \right) \\ & + p^+ \left( [\text{Fe}^{3+}] - [\text{Fe}^{3+}]_{\text{sat}} \right) \theta \left( [\text{Fe}^{3+}] - [\text{Fe}^{3+}]_{\text{sat}} \right), \end{aligned} \quad (8)$$

from the information that is known. Here,  $\theta(\cdot)$  denotes the Heaviside step function and  $[H^+]_{prec} = 10^{-3.5}$ .

This chemical system, which was kicked into action by water infiltrating pyrite-rich soil, is then left to diffuse and react. It is hypothesised that this mixing and diffusing alone is enough to form patterns of ferric hydroxide. The advection of the groundwater then assists in finalising the shape of the patterns that form.

The later event of hydrothermal alteration is not considered in this model, and it is assumed that the pattern is formed entirely at this stage in the precipitate, ferric hydroxide. The later hydrothermal alteration essentially takes that pattern, and transforms it into hematite.

### 3 Mathematical model

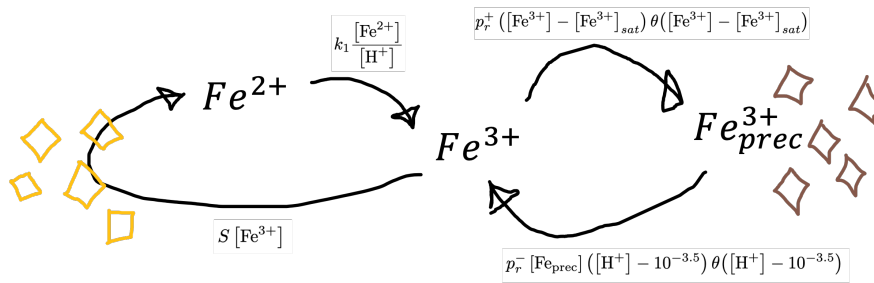


**Fig. 2** A diagram of the iron cycle present in the acid-sulfate soil system. Each reaction is presented alongside its hypothesised rate equation.

In this section, a 2D reaction-diffusion equation model is constructed to describe the chemical system in Sect. 2 following the initial pulse of  $Fe^{2+}$  and  $H^+$  ions into the soil. The model consists of five variables: the concentrations  $[Fe^{2+}]$ ,  $[Fe^{3+}]$ ,  $[H^+]$  and  $[Fe_{prec}]$  (that is, the concentration of the precipitate  $Fe(OH)_3$ ), and continuum field of microbe population  $M$ . The model will then be analysed for its ability to exhibit a Turing instability, which requires a strictly positive (in all variables) steady state in the absence of diffusion, which becomes unstable once diffusion is included. The model is presented below:

$$\frac{\partial [\text{Fe}^{2+}]}{\partial t} = -k_1 \frac{[\text{Fe}^{2+}]}{[\text{H}^+]} + \frac{15}{14}s [\text{Fe}^{3+}] - k_m [\text{H}^+] [\text{Fe}^{2+}] M + D_{\text{Fe}^{2+}} \nabla^2 [\text{Fe}^{2+}], \quad (9)$$

$$\begin{aligned} \frac{\partial [\text{Fe}^{3+}]}{\partial t} = & k_1 \frac{[\text{Fe}^{2+}]}{[\text{H}^+]} + p^- [\text{Fe}_{\text{prec}}] \left( [\text{H}^+] - [\text{H}^+]_{\text{prec}} \right) \theta \left( [\text{H}^+] - [\text{H}^+]_{\text{prec}} \right) \\ & - p^+ \left( [\text{Fe}^{3+}] - [\text{Fe}^{3+}]_{\text{sat}} \right) \theta \left( [\text{Fe}^{3+}] - [\text{Fe}^{3+}]_{\text{sat}} \right) - s [\text{Fe}^{3+}] \\ & + k_m [\text{H}^+] [\text{Fe}^{2+}] M + D_{\text{Fe}^{3+}} \nabla^2 [\text{Fe}^{3+}], \end{aligned} \quad (10)$$

$$\begin{aligned} \frac{\partial [\text{H}^+]}{\partial t} = & -k_1 \frac{[\text{Fe}^{2+}]}{[\text{H}^+]} - 3p^- [\text{Fe}_{\text{prec}}] \left( [\text{H}^+] - [\text{H}^+]_{\text{prec}} \right) \theta \left( [\text{H}^+] - [\text{H}^+]_{\text{prec}} \right) \\ & + 3p^+ \left( [\text{Fe}^{3+}] - [\text{Fe}^{3+}]_{\text{sat}} \right) \theta \left( [\text{Fe}^{3+}] - [\text{Fe}^{3+}]_{\text{sat}} \right) \\ & + \frac{8}{7}s [\text{Fe}^{3+}] - k_m [\text{H}^+] [\text{Fe}^{2+}] M - b [\text{H}^+] + D_{\text{H}^+} \nabla^2 [\text{H}^+], \end{aligned} \quad (11)$$

$$\frac{\partial M}{\partial t} = m_b [\text{H}^+] [\text{Fe}^{2+}] M - \left( m_d + m_{d[\text{Fe}^{3+}]} [\text{Fe}^{3+}] \right) M + D_M \nabla^2 M. \quad (12)$$

$$\begin{aligned} \frac{\partial [\text{Fe}_{\text{prec}}]}{\partial t} = & -p^- [\text{Fe}_{\text{prec}}] \left( [\text{H}^+] - [\text{H}^+]_{\text{prec}} \right) \theta \left( [\text{H}^+] - [\text{H}^+]_{\text{prec}} \right) \\ & + p^+ \left( [\text{Fe}^{3+}] - [\text{Fe}^{3+}]_{\text{sat}} \right) \theta \left( [\text{Fe}^{3+}] - [\text{Fe}^{3+}]_{\text{sat}} \right) \\ & - d [\text{Fe}_{\text{prec}}] + D_{\text{Fe}_{\text{prec}}} \nabla^2 [\text{Fe}_{\text{prec}}]. \end{aligned} \quad (13)$$

The rates of reaction were defined in Sect. 2, although we note that the surface reaction rate constant  $k_s$  was replaced with the constant  $s$ . This new constant describes the relevant rate of reaction, which is rate-limited by the ability of  $\text{Fe}^{3+}$  to diffuse between pyrite crystals.

There are some auxiliary terms in these equations not described by the chemical reactions alone. The first one,  $-b [\text{H}^+]$ , describes the loss of hydrogen ions as the acidity reacts with and dissolves the background soil. There is also a loss of precipitate via the term  $-d [\text{Fe}_{\text{prec}}]$ , which derives from the propensity for ferric hydroxide to react and transform into other iron oxides<sup>2</sup>. The remaining terms that require discussion are those contained within the microbial component. The term  $m_b [\text{H}^+] [\text{Fe}^{2+}] M$  represents the microbial replication term, which is aided by the presence of  $\text{Fe}^{2+}$ , as an energy source, and  $\text{H}^+$  which represents their preference for lower pH. The microbial death term,  $-\left(m_d + m_{d[\text{Fe}^{3+}]} [\text{Fe}^{3+}]\right) M$ , includes a natural cell decay coefficient  $m_d$ , and a death of bacteria due to  $\text{Fe}^{3+}$ , which is toxic to some species, that we've called  $m_{d[\text{Fe}^{3+}]}$ .

<sup>2</sup> This is probably not a great assumption to be making, but a term like this is required for a Turing instability. Turning this term into  $-d [\text{Fe}_{\text{prec}}]^2$ , however, has an interpretation as a space-wise carrying capacity (only so much precipitate can occupy one spatial unit etc...), and still permits a Turing instability.

The reaction-diffusion system is modelled on a square domain inside the  $x$ - $y$  plane of size  $[-nL, nL] \times [-nL, nL]$ . Here,  $L$  denotes a characteristic size of the pattern, and  $n$  may be adjusted to observe behaviour on larger/smaller domains that allow for additional Turing modes. The initial condition is modelled as a pulse of  $\text{Fe}^{2+}$ ,  $\text{H}^+$  and  $M$  on the negative  $x$  side of the  $x$ - $y$  plane, which we define by

$$\begin{aligned} [\text{Fe}^{2+}]|_{t=0} &= [\text{Fe}^{2+}]_0 \left( 1 + \frac{\cos(\frac{\pi}{nL}y)}{10} \right) \left( \frac{4}{5} - \frac{3 \sin(\frac{\pi}{2nL}x)}{5} \right), \\ [\text{Fe}^{3+}]|_{t=0} &= 0, \\ [\text{H}^+]|_{t=0} &= [\text{H}^+]_{\text{prec}} \left( 1 + \frac{\cos(\frac{\pi}{nL}y)}{10} \right) \left( 2 - 1.99 \sin\left(\frac{\pi}{2nL}x\right) \right), \quad (14) \\ [\text{Fe}_{\text{prec}}]|_{t=0} &= 0, \\ M|_{t=0} &= M_0 \left( 1 + \frac{\cos(\frac{\pi}{nL}y)}{10} \right) \left( \frac{3}{5} - \frac{\sin(\frac{\pi}{2nL}x)}{10} \right). \end{aligned}$$

Values for all dimensional parameters are given in table 1. To obtain a dimensionless model, we non-dimensionalise according to the scales defined in table 2. These non-dimensionalisations yield the dimensionless groups given in table 3. With respect to these non-dimensionalisations, and ignoring terms that are small, our model (9)-(13) reduces to

$$c_{2,h} \frac{\partial f_2}{\partial \tau} = -K_1 \frac{f_2}{h} + \frac{15}{14} S f_3 - K_m h f_2 m + D_{2,h} \tilde{\nabla}^2 f_2, \quad (15)$$

$$\begin{aligned} c_{3,h} \frac{\partial f_3}{\partial \tau} &= K_1 \frac{f_2}{h} + f_{\text{prec}} (h-1) \theta(h-1) - P (f_3-1) \theta(f_3-1) \\ &\quad - S f_3 + K_m h f_2 m, \end{aligned} \quad (16)$$

$$\begin{aligned} \frac{\partial h}{\partial \tau} &= -K_1 \frac{f_2}{h} - 3 f_{\text{prec}} (h-1) \theta(h-1) + 3P (f_3-1) \theta(f_3-1) \\ &\quad + \frac{8}{7} S f_3 - K_m h f_2 m - B h + \tilde{\nabla}^2 h, \end{aligned} \quad (17)$$

$$\frac{\partial m}{\partial \tau} = M_b h f_2 m - M_d m, \quad (18)$$

$$c_{p,h} \frac{\partial f_{\text{prec}}}{\partial \tau} = -f_{\text{prec}} (h-1) \theta(h-1) + P (f_3-1) \theta(f_3-1) - D f_{\text{prec}}. \quad (19)$$

It can be observed now, from table 3, that most of the chemical reactions occur at rates of similar orders of magnitude, and thus we are justified in including all of them. The one reaction, however, which occurs much slower, is the rate-limiting reaction corresponding to  $K_1$ . This reaction is still kept in the model, however, as it becomes significant in regions where  $\text{H}^+$  concentration drops and is the preferred  $\text{Fe}^{2+}$  oxidation pathway (rather than the microbes). The results obtained from this model will be shown in Sect. 4.

**Table 1** Dimensional parameter values

Parameter	Value	Notes
$L$	$5 \times 10^{-2}$	5 cm, the average size of the pattern bed
$k_1$	$5.8 \times 10^{-11} [\text{Fe}^{2+}]_0$	Obtained by comparing to the low pH results of [9]
$s$	$1.5 \times 10^{-4}$	The reciprocal of the time-scale for diffusion of $\text{Fe}^{3+}$ between pyrite crystals
$p^-$	0.13	Estimated from the solubility table of [5]
$p^+$	$1.2 \times 10^{-3}$	Estimated from the half-life of $\text{Fe}(\text{OH})_3$ in [7]
$k_m$	$1.9 \times 10^{10}$	Obtained from Andrew Coward's slides. Units unknown
$b$	$1.4 \times 10^{-7}$	Estimated from the dissolution of kaolinite in acidic systems [8]
$m_d$	$3.9 \times 10^{-6}$	Estimated by assuming lifespan of a microbe is 3 days
$m_b$	$> \frac{1.3 \times 10^{-2}}{[\text{Fe}^{2+}]_0}$	Estimated by comparison with microbe death rate
$m_d[\text{Fe}^{3+}]$	Unknown	Assumed to be about an order of magnitude lower than $m_d$ and thus will be ignored in further analysis
$d$	$2.8 \times 10^{-6}$	Estimated from the solubility table of [5]
$[\text{H}^+]_{\text{prec}}$	$10^{-3.5}$	Ferric hydroxide insoluble above a pH of 3.5 (from Andrew Coward's slides)
$K_{sp}$	$10^{-3.54}$	From [2]
$[\text{Fe}^{3+}]_{\text{sat}}$	$1.1 \times 10^{-7}$	Obtained from the solubility equilibrium for $\text{Fe}^{3+}$ ; $K_{sp} = \frac{[\text{Fe}^{3+}]}{[\text{H}^+]^3_{\text{prec}}}$
$D_{\text{Fe}^{2+}}$	$7.2 \times 10^{-10}$	From [2]
$D_{\text{Fe}^{3+}}$	$6.1 \times 10^{-10}$	From [2]
$D_{\text{H}^+}$	$9.3 \times 10^{-9}$	From [2]
$D_M$	Unknown	Most acidophilic bacteria are very weakly motile, so we assume this is small and ignored in further analysis
$D_{\text{Fe}_{\text{prec}}}$	$\sim 0$	Probably very small because this is a precipitate, so ignored in further analysis
$[\text{Fe}^{2+}]_0$	$\sim 10^{-2} - 10^{-4}$	Initial concentration of $\text{Fe}^{2+}$ after waterlogging event unknown; depends on how much pyrite was in the soil. Potential range given
$M_0$	$\sim \frac{1.7 \times 10^{-18}}{[\text{Fe}^{2+}]_0}$	Unsure. Estimated by balancing with the surface reaction term $S$

## 4 Pattern formation

In this section, some results are discussed and the model is simulated for some values within a regime that permits a Turing instability.

In order to test our hypothesis that the pattern was formed during the waterlogging event, we require that the model (15)-(19) admit a Turing instability. For this to occur, we require that the (strictly) positive steady state of (15)-(19) is stable in the absence of diffusion, and that this steady state becomes unstable when diffusion is included. Finding the criterion for stability—and then the additional criterion for Turing instability—for a non-linear five-parameter system is rather cumbersome.

**Table 2** Choice of characteristic values for variables

Dimensionless Variable	Variable	Scale	Notes
$\tilde{\nabla}$	$\nabla$	$\frac{1}{L}$	Both spatial dimensions are $\mathcal{O}(L)$ Using timescale for diffusion of $H^+$ across the length $L$
$\tau$	$t$	$\frac{L^2}{D_{H^+}}$	
$f_2$	$[Fe^{2+}]$	$[Fe^{2+}]_0$	Natural scale that emerges from the non-dimensionalisation
$f_3$	$[Fe^{3+}]$	$[Fe^{3+}]_{sat}$	
$h$	$[H^+]$	$[H^+]_{prec}$	
$m$	$M$	$M_0$	
$f_p$	$[Fe_{prec}]$	$\frac{D_{H^+}}{L^2 p^-}$	

**Table 3** Dimensionless groups

Dimensionless group	Definition	Value
$K_1$	$\frac{k_1 [Fe^{2+}]_0 L^2}{D_{H^+} [H^+]_{prec}^2}$	$155.8 [Fe^{2+}]_0^2$
$S$	$\frac{s K_{sp} [H^+]_{prec}^2 L^2}{D_{H^+}}$	0.014
$P$	$\frac{p^+ K_{sp} [H^+]_{prec}^2 L^2}{D_{H^+}}$	0.108
$K_m$	$\frac{k_m [Fe^{2+}]_0 M_0 L^2}{D_{H^+}}$	0.0085
$B$	$\frac{b L^2}{D_{H^+}}$	0.037
$M_b$	$\frac{m_b [H^+]_{prec} [Fe^{2+}]_0 L^2}{D_{H^+}}$	1.036
$M_d$	$\frac{m_d L^2}{D_{H^+}}$	1.036
$D$	$\frac{d}{p^- [H^+]_{prec}}$	0.068
$D_{2,h}$	$\frac{D_{Fe^{2+}} [Fe^{2+}]_0}{D_{H^+} [H^+]_{prec}}$	$244.2 [Fe^{2+}]_0$
$c_{2,h}$	$\frac{[Fe^{2+}]_0}{[H^+]_{prec}}$	$3162.28 [Fe^{2+}]_0$
$c_{3,h}$	$K_{sp} [H^+]_{prec}^2$	0.00035
$c_{p,h}$	$\frac{D_{H^+}}{L^2 p^- [H^+]_{prec}}$	0.009

some; applying the Routh-Hurwitz criteria to obtain this region of parameter space yields formulae far too large to include in this report. It was more worthwhile testing guesses of parameter values to see if the stability criterion was satisfied, and afterwards observing if the conditions for a Turing instability could be satisfied. Upon substituting the values of the dimensionless groups in table 3 into the model (15)-(19), we do not see a stable steady state, let alone a Turing instability. More careful estimation of the parameters, then, is required to confirm whether a Turing instability occurred in reality.

However, some guessed values were found that permitted Turing instabilities. It was also observed that two possible positive steady states could exist: one with  $h > 1$  and one with  $h < 1$ , each giving qualitatively different patterns.

In order to simulate this model, a numerical solver was written based on the spectral algorithm in [4] involving the solution on Fourier modes. This algorithm worked fast, but with the downside of imposing periodic boundary conditions. This still allowed us to see patterns, though it doesn't model the physical boundary conditions occurring along the rock bed. The solver was run until the patterns had settled forming. Figures 3, 4, 5 are plots of the final, stable patterning found, along with the parameter values that yielded them.

We reproduce many types of the observed zebra rock patterns, including an important hallmark of the pattern, wherein the highest concentration of hematite occurs at the rim of the red banding [3]. Even on an entirely periodic domain, patterns involving both spots and stripes have been observed. A significant type of pattern has not been seen in simulations, however, which is that of the 'halos' of the Duncan Road zebra rock samples. This morphology is possibly representative of a secondary instability which created more hematite at a later time, a long time-scale effect due to the slow dissolution of the pyrite crystal, or an artifact of correct boundary conditions or 3D diffusion.

## 5 Conclusion and future work

We have been able to model the iron precipitation reaction chain, which occurred as a result of waterlogging pyrite-rich soil, as a reaction-diffusion equation supplemented with appropriate boundary conditions. Using the model we constructed, the capacity for a Turing instability is found, and this instability replicates the majority of the patterns observed on real zebra rock samples. However, the real parameter values we estimated for each rate of reaction do not give rise to a Turing instability, and our model does not reproduce the 'halo' pattern observed in Duncan Road samples.

To extend this research, more work must be done to figure out the rates of reaction, and the exact kinetics of more complicated reactions, under these environmental conditions. The research into the precipitation reaction and microbial interactions in particular were not conclusive. Ideally, with this knowledge, we may be able to determine finally if the zebra rock pattern formed as a result of a Turing instability.

The author would also like to thank his supervisor, A/Prof Anja Slim, for proposing such an interesting project, and for being so generous with her time and help over the three-week program and beyond.

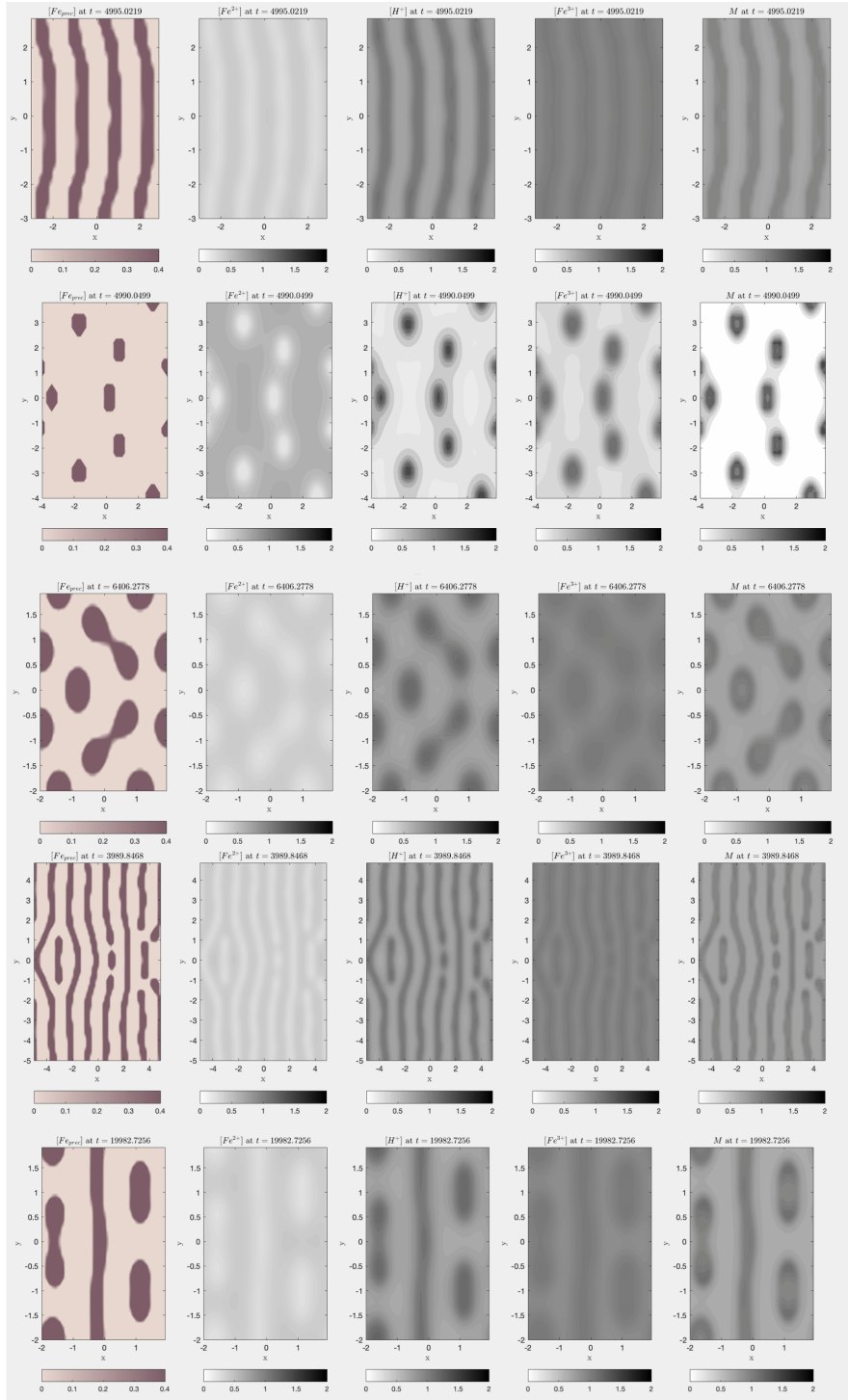


**Fig. 3** Pattern results for  $K_1 = 0.3$ ,  $S = 0.25$ ,  $K_m = 1$ ,  $P = 4$ ,  $B = 0.08$ ,  $M_b = 0.5$ ,  $M_d = 0.2$ ,  $D = 0.1$ ,  $c_{2,h} = 1$ ,  $c_{3,h} = 1$ ,  $c_{p,h} = 1$  while we vary  $n$  (the domain size), and vary  $D_{2,h}$  above its Turing threshold of 1.3.

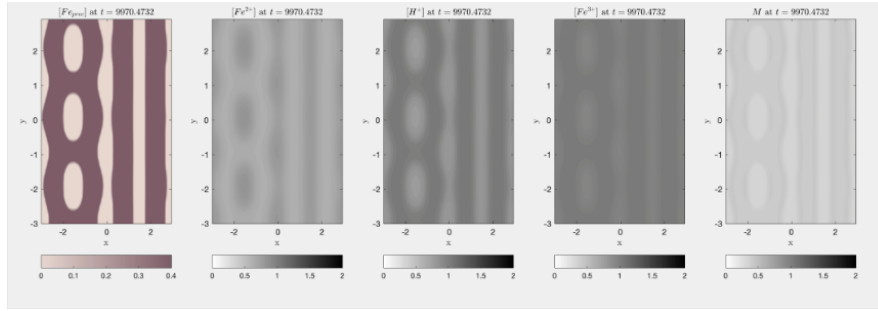


**Fig. 4** Pattern results for a separate set of parameters;  $K_1 = 0.4$ ,  $S = 0.27$ ,  $K_m = 1$ ,  $P = 2$ ,  $B = 0.08$ ,  $M_b = 0.45$ ,  $M_d = 0.1$ ,  $D = 0.05$ ,  $c_{2,h} = 1$ ,  $c_{3,h} = 1$ ,  $c_{p,h} = 1$ ,  $D_{2,h} = 3$ , recovering a zebra that is black with white stripes!

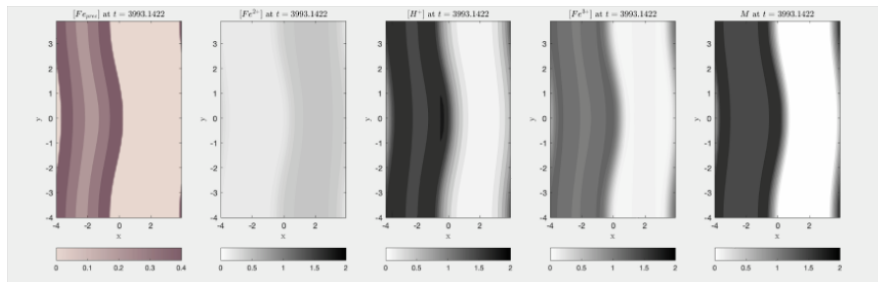


**Fig. 5** Pattern results for a separate set of parameters, where the steady state has  $h > 1$ ;  $K_1 = 0.3$ ,  $S = 0.4$ ,  $K_m = 1$ ,  $P = 2$ ,  $B = 0.08$ ,  $M_b = 0.5$ ,  $M_d = 0.1$ ,  $D = 0.1$ ,  $c_{2,h} = 1$ ,  $c_{3,h} = 1$ ,  $c_{p,h} = 1$ ,  $D_{2,h} = 5$ , which gives an interest bi-stability pattern.

## References

1. Abrajevitch, A., Pillans, B.J., Roberts, A.P., Kodama, K.: Magnetic properties and paleomagnetism of zebra rock, western australia: Chemical remanence acquisition in hematite pigment and ediacaran geomagnetic field behavior. *Geochemistry, Geophysics, Geosystems* **19**(3), 732–748 (2018)
2. Coward, A.J.: How the zebra rock got its stripes: the formation of hematite banding in western australian siltstones. Ph.D. thesis, Monash University (2022)
3. Coward, A.J., Slim, A.C., Brugger, J., Wilson, S., Williams, T., Pillans, B., Maksimenko, A.: Mineralogy and geochemistry of pattern formation in zebra rock from the east kimberley, australia. *Chemical Geology* **622**, 121,336 (2023)
4. Craster, R.V., Sassi, R.: Spectral algorithms for reaction-diffusion equations. arXiv preprint arXiv:1810.07431 (2018)
5. Furcas, F.E., Lothenbach, B., Isgor, O.B., Mundra, S., Zhang, Z., Angst, U.M.: Solubility and speciation of iron in cementitious systems. *Cement and Concrete Research* **151**, 106,620 (2022)
6. Geidans, L.: zebra rock of western australia. In: Geological Society of Australia, Abstracts, vol. 3 (1981)
7. Grundl, T., Delwiche, J.: Kinetics of ferric oxyhydroxide precipitation. *Journal of Contaminant Hydrology* **14**(1), 71–87 (1993)

8. Huertas, F.J., Chou, L., Wollast, R.: Mechanism of kaolinite dissolution at room temperature and pressure part ii: Kinetic study. *Geochimica et cosmochimica acta* **63**(19-20), 3261–3275 (1999)
9. Iwai, M., Majima, H., Izaki, T.: A kinetic study on the oxidation of ferrous ion with dissolved molecular oxygen. *Denki Kagaku oyobi Kogyo Butsuri Kagaku* **47**(7), 409–414 (1979)
10. Kumar, M., Zeyad, M.T., Choudhary, P., Paul, S., Chakdar, H., Rajawat, M.V.S.: Thiobacillus. In: *Beneficial microbes in agro-ecology*, pp. 545–557. Elsevier (2020)
11. Turing, A.M.: The chemical basis of morphogenesis. *Bulletin of mathematical biology* **52**, 153–197 (1990)